A Novel X-ray Diffractometer to Study the Texture of Materials

C. C. Tang,[a] M. C. Miller,[a] S. M. Clark,[a] M. A. Player[b] and G. R. G. Craib[b]

[a]Daresbury Laboratory, Warrington, Cheshire WA4 4AD, UK, and [b]Department of Engineering, University of Aberdeen, Aberdeen AB9 2UE, UK

An X-ray energy-dispersive diffraction technique to study the texture of materials using synchrotron radiation has been developed. The design and commissioning of the diffraction instrument are described. The technique was first applied to study a drawn-wire aluminium sample which has a well known deformation texture. To demonstrate its capability further, results obtained from an erbium evaporated thin film are also presented.

1. Introduction

The properties of polycrystalline preferred orientation or texture are of great technological importance in solids. Aggregation is a very common condition in natural and manufactured materials. In metals and alloys it is most evident in wires, sheets and on surfaces. As the properties of materials are correlated to their textures, they have been intensively studied by X-ray diffraction methods for many years. To provide a convenient means for presenting such results, stereographic projections or *pole figures* have been used. A pole figure is the pole density variation of pole orientation for a set of crystal planes, with respect to a specific orientation of the specimen. Texture information is therefore essential to materials science, engineering, geology, metallurgy and mineralogy. For information on deformation and recrystallization textures in wire and sheet form, readers are referred to Dillamore & Roberts (1965) and Barrett & Massalski (1966).

Although conventional techniques of texture analysis using monochromatic radiation and point-by-point scanning are important and widely used, they are also time consuming. General reviews of these techniques are given by Cullity (1978) and Klug & Alexander (1974). With increasing production of new and exciting materials from academia and industry, we were motivated to devise an alternative faster technique. Indeed, an exploratory fast data-collection technique using an energy-dispersive powder diffraction (EDPD) camera on an X-ray synchrotron source has been reported previously (Cernik, Clark & Pattison, 1989; Player, Marr, Gu, Savaloni, Öncan & Munro, 1992). Preliminary pole figures obtained from an Er film demonstrated the potential of this method. We have subsequently constructed a new diffraction rig which employs white synchrotron X-rays and energy-dispersive powder diffraction to yield texture information rapidly. To demonstrate the viability of this apparatus, we have obtained results from an Al wire, which is expected to have a fibre texture. For texture analysis of a thin film, we used a 600 nm Er specimen deposited by UHV evaporation on Mo substrates. The design and implementation of this new technique are described in the subsequent section.

2. Instrumentation

A diffraction rig has been designed and built for texture or pole-figure measurements using flat-plate or wire specimens. The diffractometer was implemented on the energy-dispersive set-up of station 9.7 at the Daresbury Synchrotron Radiation Source (SRS). More details of the energy-dispersive powder diffraction instrument are given by Clark (1989, 1992). The station receives X-radiation from a 5 T superconducting wiggler magnet located in the 2 GeV ring which stores an electron beam with a typical current of 200 mA. The emergent X-rays are linearly polarized in the horizontal plane. The useful flux has energies ranging from 10 to 100 keV with a peak intensity of ca 10^{12} photons s^{-1} mm^{-2} in 0.1% bandwidth at 10 keV.

The principal objective of the experimental design was to allow a sample to be examined in as many orientations as possible. The device consists of two rotary tables (ω and φ) and two arcs (α and ψ), as shown schematically in Fig. 1. The ω-circle is mounted with its rotational axis vertical, and is currently used for alignment only. Directly above this is the ψ-circle which provides sample rotation (roll) of 0–90° about the incident beam. This axis can alternatively be offset by 45° to give an angular range of ±45°. Sitting above the ψ-circle is the α-circle which defines the angle of X-ray incidence; it has an angular range of ±45°. When the arcs are at their zero positions, the rotational axis of the φ-circle (on top of the α-circle) is parallel to the rotation axis of the ω table.

This diffraction arrangement was first used by Player *et al.* (1992). If the positions of ψ and α were reversed, then the geometry would be that used by Heizmann, Vadon, Schlatter & Bessières (1988). The two geometries require different formulae for intensity and position corrections, as discussed by Player *et al.* (1992). Both arrangements allow low glancing angles of α to be used, thereby increasing sensitivity to thin surface layers (relative to the standard symmetrical Bragg–Brentano reflection geometry in which α is equal to the Bragg angle θ), and both suffer from a central 'blind spot' of radius $\alpha - \theta$, near the pole of the stereographic projection, corresponding to the sample normal. The difference between them is that in the arrangement of Heizmann *et al.* (1988) the axis of the ψ-rotation is inclined at the angle α to the synchrotron radiation beam and lies in the plane of the sample surface, while in the arrangement of Player *et al.* (1992) the ψ-axis coincides with the beam and the sample surface is inclined at α to this axis. As a result, in the arrangement of Player *et al.* (1992) the beam footprint on the sample remains constant as ψ is varied, and the intensity correction factor is nearer constant for very thin film samples. However, the arrangement of Heizmann *et al.* (1988) in principle permits operation out to higher values of ψ (although the difference is small for small values of α) and gives a near constant correction factor for thick samples; it also reduces to the Bragg–Brentano arrangement at $\alpha = \theta$, which is not the case in the arrangement of Player *et al.* (1992) (contrary to a remark in the paper). In summary, the general arrangement of Player *et al.* (1992) adopted in the present instrument is considered advantageous for very thin film specimens, or where low α is used to achieve surface sensitivity, or where a constant beam footprint is desirable. However, the arrangement of Heizmann *et al.* (1988) may be advantageous for thick samples particularly at or near the Bragg–Brentano condition.

Fig. 2 is a photograph of the diffractometer taken in plan-side view. The apparatus is *ca* 30 cm in diameter and 25 cm in height, and it weighs *ca* 12 kg. The tables and

Figure 1
Schematic representation of the diffraction geometry.

arcs are driven by stepper motors to allow each axis to be positioned with an accuracy better than 0.1°. A built-in telescope, which can swivel in the horizontal plane, is used for sample alignment. A copper sheet sample is visible in this photograph. The incident beam is reduced in size by a series of slits and emerges from the beam pipe (identified by yellow shielding). It is then further defined by a 0.5 or 1.0 mm diameter collimator before reaching the sample. Use of slits in the beam pipe, and close positioning of the collimator to the beam-pipe exit window, serve to reduce any scattering from the surroundings.

The diffracted beam is detected by an EG&G Ortec intrinsic germanium solid-state detector with an energy resolution of $\Delta E/E \simeq 0.005$ at 30 keV. A fixed diffraction angle 2θ is defined by a set of multiple slits with an aperture of 5 mm height and 10 mm width. The slits consist of 50 × 500 mm long parallel foils, each 50 μm thick and separated by 50 μm. Use of multiple slits increases the diffracting area without affecting overall momentum resolution. The diffracted photons are then electronically resolved in energy by a multi-channel analyser (MCA). Intensity peaks correspond to each set of lattice planes of interplanar spacing d (Å) in the crystalline sample, diffracting X-rays of energy E, given by E (keV) = $6.199/(d\sin\theta)$. The data-collection software has been set up so that a series of intensity–energy spectra are recorded as the sample orientation is varied. Data acquisition is described in the next section.

3. Data acquisition

The control system is based on the *PINCER* data-acquisition software (Miller, Ackroyd & Oszlanyi, 1994) which is now in widespread use on several SRS experimental stations. The software is based on a powerful command interpreter and provides a large suite of functions that can be readily combined in 'macro' command files. On station 9.7, *PINCER* runs on a Viglen AT-bus personal computer which has a Hytec Electronics 1330 interface to a single CAMAC instrument crate which houses cards for stepper motor, counter-timer and multi-channel analyser operations. These are all of Daresbury design with the exception of a LeCroy spectroscopic analogue-to-digital converter (ADC). Fig. 3 shows a schematic representation of the data-acquisition facility. All motors, including those on the diffractometer, are driven from a single NE9100 stepper motor multiplexer card which can drive an axis selected by an 8-bit address set on a daisy-chained highway interface module (HIM).

The timing is carried out by an EC728 time-frame generator which can specify up to 512 pairs of data-collection and wait periods (frames) in the range 16 μs to 2560 s. It provides both LEMO control signals and a 10-bit frame number *via* a front panel ribbon connector. This allows real time and autonomous operation of both the 32-channel scaler EC727 and the multi-channel analyser with data being stored in a local CAMAC memory until later read out by the host computer. The EC727 accepts TTL signals from a reference pulse generator, ion chamber, beam
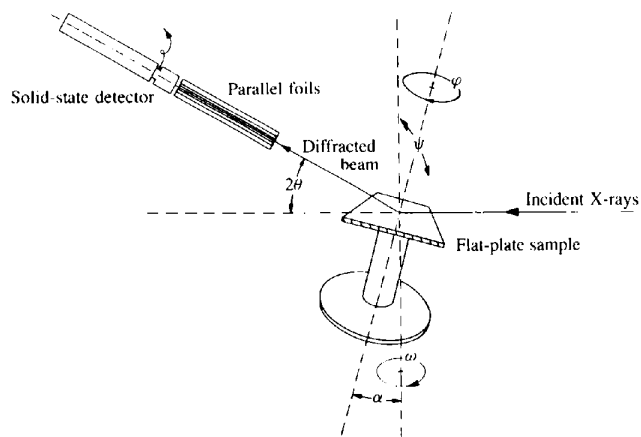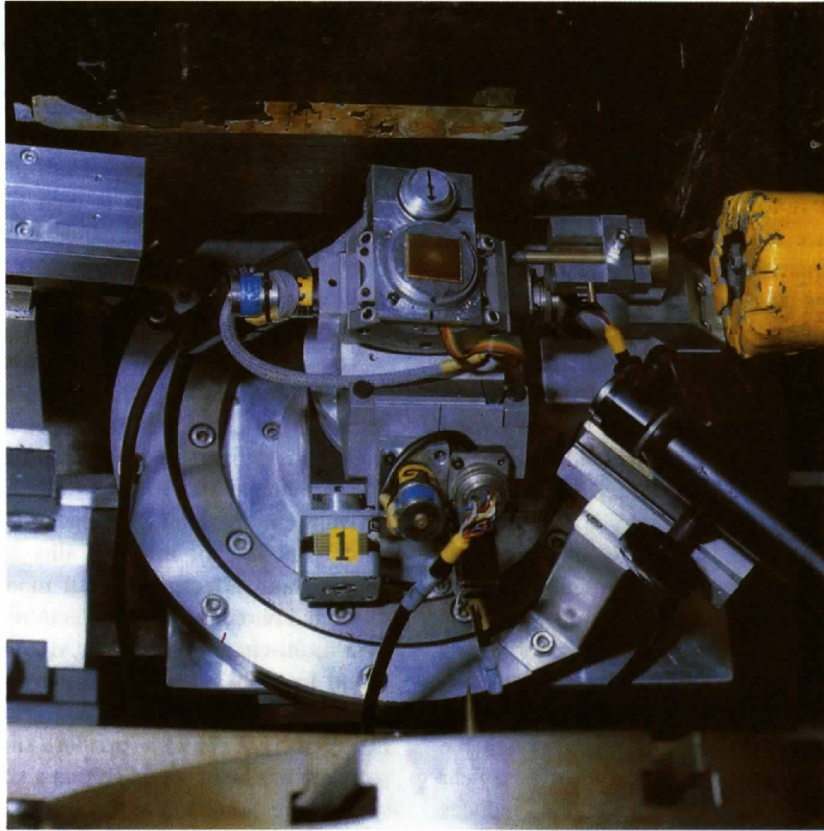
Figure 2
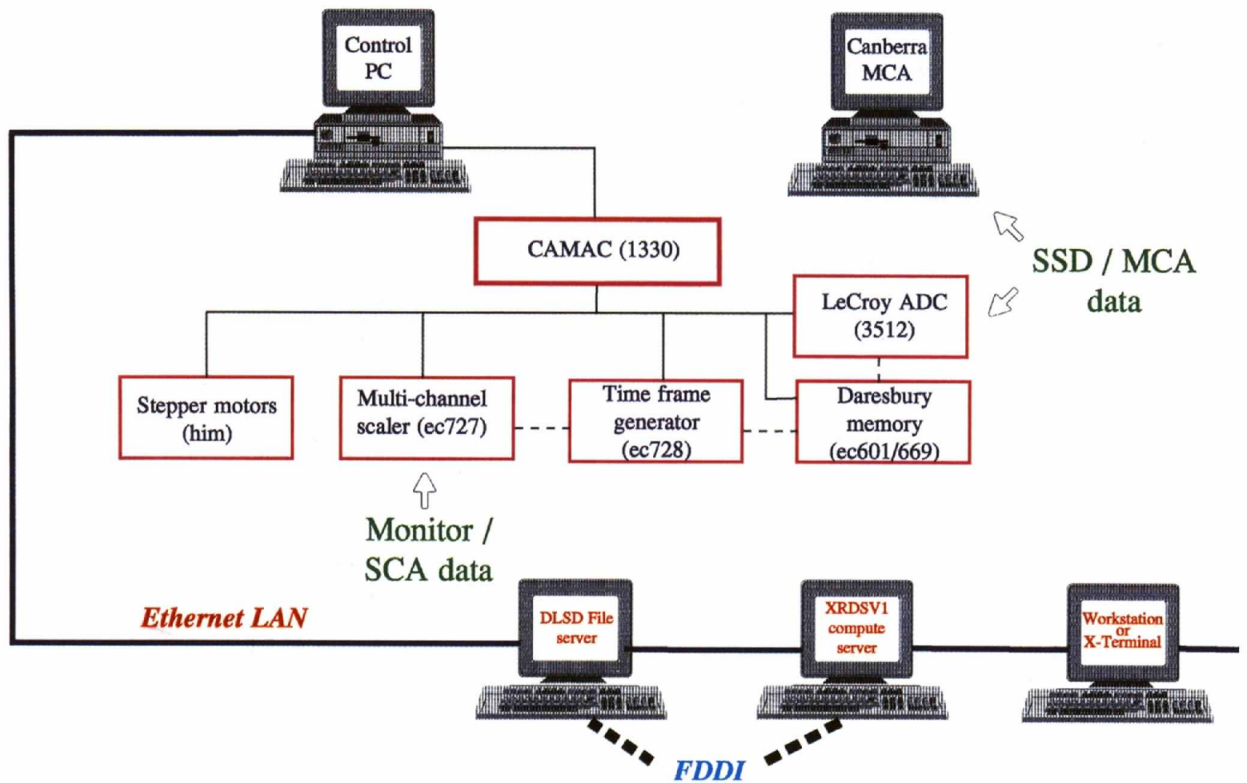Photograph of the diffraction apparatus.

Figure 3
Pole-figure data-acquisition facility in schematic form.

monitor and a number of single-channel analysers (SCA). These are set to integrate total multi-channel analyser counts together with six selected regions of interest (Clark & Miller, 1990).

The multi-channel analyser is based on an EC601 Daresbury memory controller with 3 Mbytes memory of 24 bits per channel (EC669) allowing up to 512 spectra to be collected in CAMAC memory *via* a private bus. A LeCroy 3512

ADC in 12-bit mode converts the pulse derived from the solid-state detector after shaping and amplification into a voltage proportional to the incident X-ray photon energy. This is then passed *via* a 3588 histogramming memory bus to an EC652 TDC combiner module. This then derives a channel address based on the converted voltage and the current frame number from the time-frame generator which is then incremented by the EC601. This process can result in 4000 channel real-time spectra being collected in the multi-channel analyser corresponding to successive live frames. A second PC runs the Canberra S100 multi-channel analyser system which is user friendly but a low-performance way of monitoring and setting up the multi-channel analyser, and includes selection of the regions of interest.

The software of the pole-figure macro itself does not need to make use of the full kinetic mode functionality of the multi-channel analyser. During the scan it successively positions two selected motors to specified real-space positions and collects data for a single live frame of the selected time duration using the minimum dead-frame period. The multi-channel analyser spectrum and scaler counts are then read from the CAMAC EC601/EC669 and EC727 memories, respectively, and written to an ASCII data file during the next live frame period. After scan completion, the files are sent *via* the 10 Mbits s⁻¹ site Ethernet to a queue for long-term storage on magneto-optical disk.
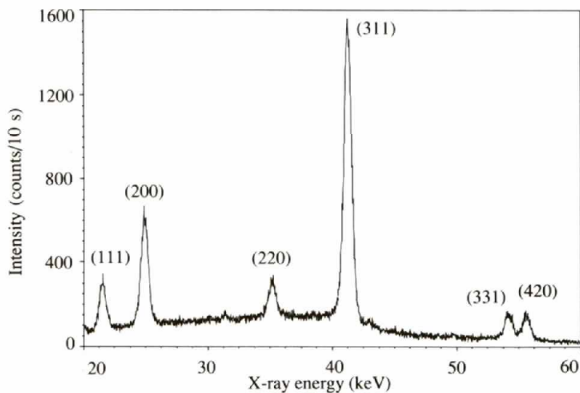

Figure 4
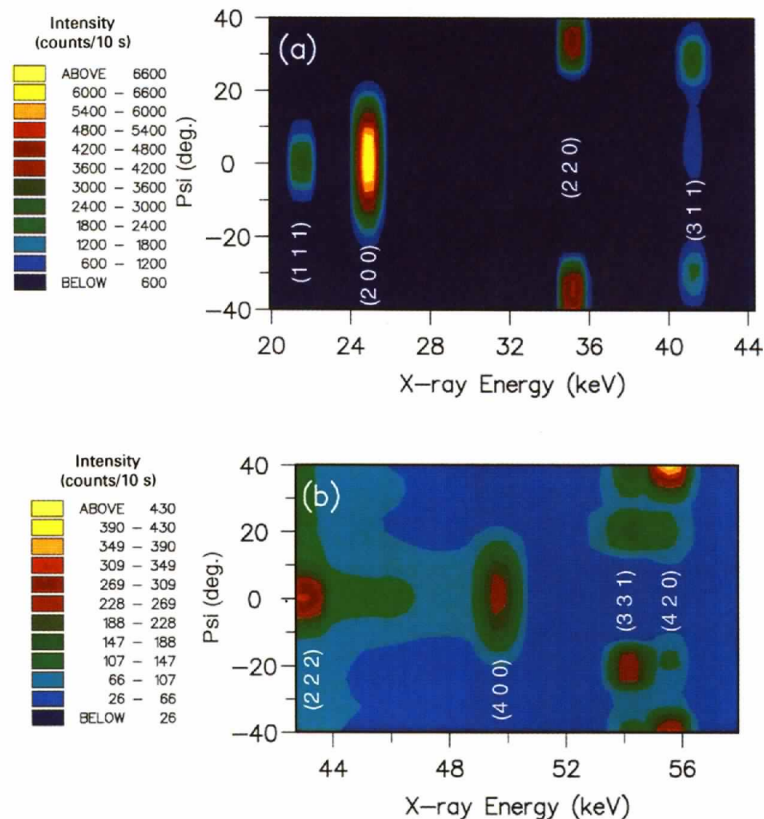Energy-dispersive diffraction pattern of Al wire taken at $\psi = 24°$ and $\varphi = 0°$.

Figure 5
Texture mapping for the Al wire: (*a*) low X-ray energy; (*b*) high X-ray energy. The intensity scale in (*b*) has been set in order to enhance the weaker features.

They are available for rapid access, for a period, *via* a 100 Mbits s^{-1} FDDI link from the SG Challenge L compute server machine. This is part of the project distributed computing 'village' which also provides VAX/VMS support and links to Internet/JANET for remote file transfer.

4. Experiments

A 1.0 mm diameter and 10 mm long Al sample was mounted with the wire axis vertical and at the centre of rotation of the diffractometer, *i.e.* in the scattering plane when $\psi = 0°$. An incident beam of 1.0 mm diameter

illuminated the cross section of the wire. With this arrangement, we can readily analyse the fibre texture with a series of discrete positions of the ψ-circle alone. In contrast, the Er thin film was mounted with its surface normal in the scattering plane when $\psi = 0°$. With the sample in this geometry, the texture can be analysed by scanning the φ- and ψ-circles. To optimize the number and position of diffraction peaks, the detector angle was manually adjusted to be at *ca* 14 and 10° for the wire and the thin film measurements, respectively. For the Al sample, the α-circle was set to half of the value of the detector angle, while for the Er film a value of $\alpha = 2°$ was used.
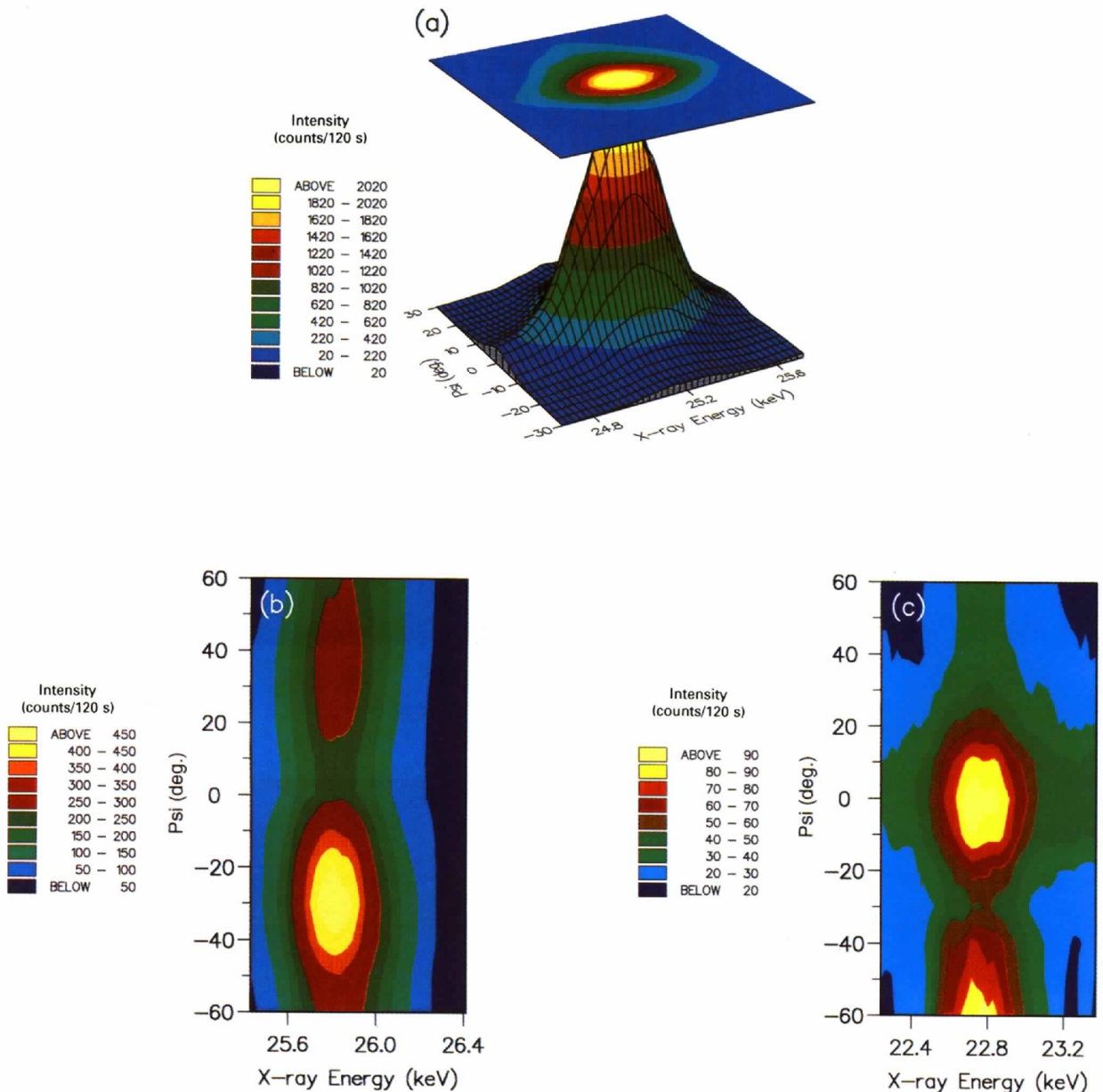

Figure 6
Texture mapping of Er thin film on Mo substrate deposited at $T_s = 573$ K. Maps taken at $\varphi = 0°$: (*a*) (002) reflection as three-dimensional plot and projective map; (*b*) (101) reflection; (*c*) (100) reflection.

The Er thin film was deposited by electron-beam evaporation onto an Mo sheet substrate at substrate temperature $T_s = 573$ K under UHV conditions, and has a nominal thickness of 600 nm. It was produced as part of a programme of research into the microstructure and texture of evaporated polycrystalline thin films and the dependence on deposition conditions. As reported by Player *et al.* (1992), the texture of such films is of approximately fibre or mixed-fibre type and depends markedly on the substrate temperature. The films are most highly oriented at mid-temperatures, corresponding to the middle of Zone II of the Structure Zone Model.

5. Results

Fig. 4 shows the energy-dispersive diffraction pattern collected in 10 s from the Al wire set in one particular orientation. Note that this single pattern contains a large number of reflections from the f.c.c. crystallites in the sample. To build a complete picture of the orientation–intensity dependence, we scanned the ψ-circle from −40 to +40° with a step of 2°. Figs. 5(a) and 5(b) were obtained in about half an hour and they clearly show that the sample possesses a double fibre texture [111] + [100] as is well known for drawn wire (see, for example, Cullity, 1978). Most of the expected interplanar angles can be identified on the maps. For instance, the angle between $\langle 111 \rangle$ and $\langle 111 \rangle$ is 0°, $\langle 111 \rangle$ and $\langle 110 \rangle$ is 35°, and that between $\langle 100 \rangle$ and $\langle 100 \rangle$ is 0°. However, the intense region at $\psi = 0°$ for the (311) reflection does not correspond to the fibre texture. Possibly, the deeper X-ray penetration at this energy (42 keV; $1/\mu \simeq 6.5 \times 10^3$ μm) reveals an additional preferred alignment. The broad feature between 44 and 48 keV is clearly not associated with the f.c.c. structure and its origin is not understood.
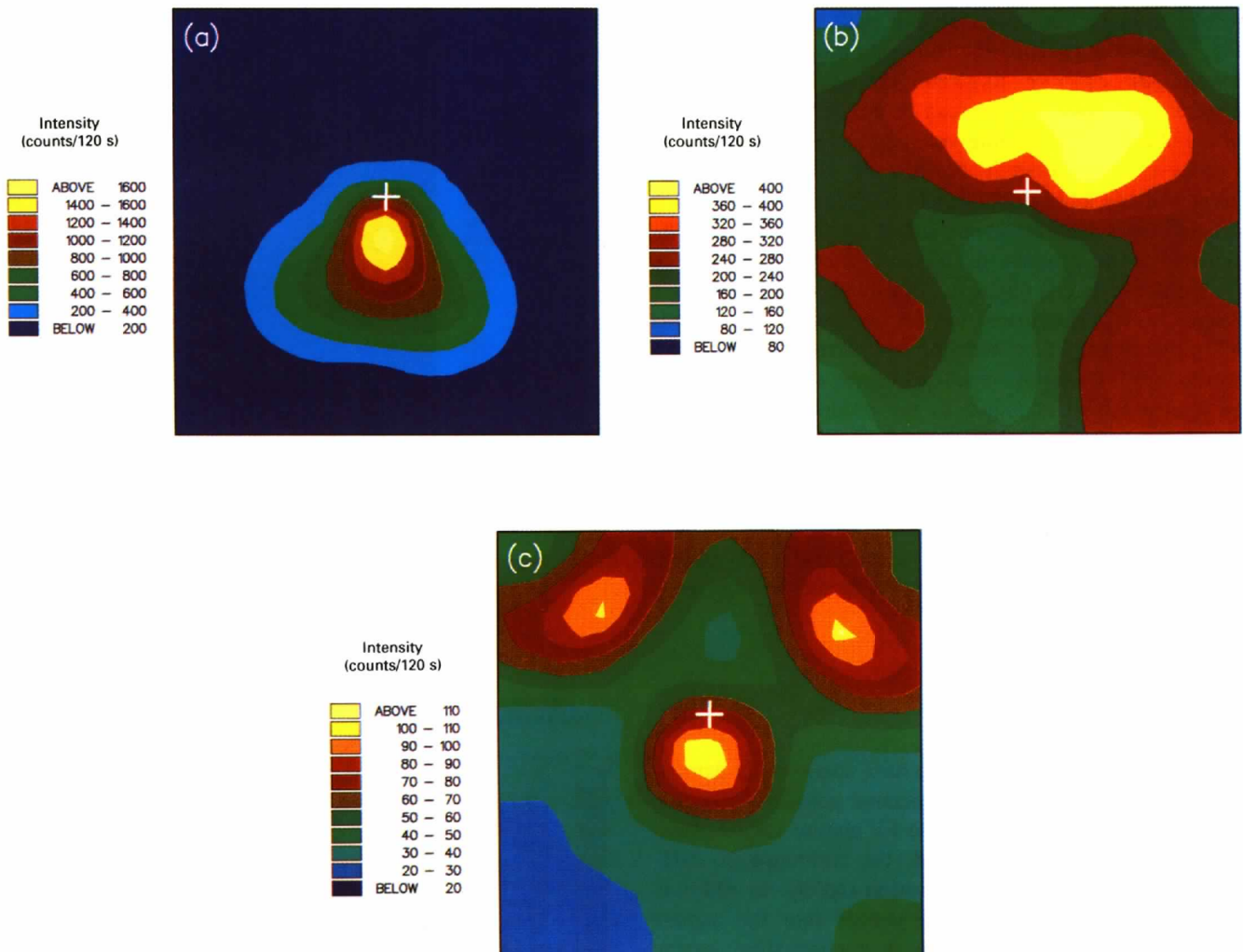

Figure 7
Pole figure of Er film, with vapour incidence (at 8.5° to normal) shown by the cross: (a) (002) reflection; (b) (101) reflection (intensity × 4); (c) (100) reflection (intensity × 15). Stereographic projections in this and subsequent figures are centred on the sample normal and extended out to $\iota = 60°$ at the midpoints of the square boundary.

Fig. 6(a) is a three-dimensional plot with projective intensity mapping of the (002) reflection for the Er thin film taken at $\varphi = 0°$. The intensity maps of (101) and (100) reflections taken at the same φ angle are presented in Figs. 6(b) and 6(c), respectively. Figs. 7(a), 7(b) and 7(c) show the (002), (101) and (100) pole figures, respectively. These and subsequent pole figures are plotted as stereographic projections centred on the sample normal, and extend out to $\psi = 60°$ at the mid-points of the square boundary. The dominant [002] orientation, with some [100] admixture, is apparent. However, the angle between the (002) and (101) poles is less than the crystallographic angle of approximately 61° for h.c.p. erbium, and the (101) pole intensity is strongly asymmetrical with respect to the sample normal, indicating a real departure from simple fibre texture.

The pole figures are shown without intensity correction: the general effect of roll angle ψ on the intensity is shown by the Mo substrate fluorescence in Fig. 8, which also demonstrates the rotational symmetry of the diffractometer. The rapid fall-off in intensity at values of ψ beyond *ca* 45° results from the very oblique exit path through the film. Fig. 9 shows the (110) simultaneously acquired pole figure for the Mo substrate, illustrating its expected sheet-type texture. Intensity correction can be applied to take account of the changes in scattering volume and of absorption with varying ψ, as described by Player *et al.* (1992); the change in intensity of substrate fluorescence with varying ψ, which results from similar effects including absorption in the film, can be used to estimate the absorption coefficient needed for the correction, if required. As the variation of substrate fluorescence is dominated by the film absorption, it falls off more rapidly than the film diffracted intensity with increasing ψ. Using the results of Player *et al.* (1992) with an optical thickness (equal to the product of absorption coefficient and physical thickness) of 0.1, the diffraction intensity correction factor for this film is estimated to be approximately 1.31 at $\psi = 60°$, while the fluorescence is estimated to fall by a factor 4.38. Accordingly, the effect of intensity correction on the pole figures is relatively minor. For further discussion on correction factors the reader is referred to Player *et al.* (1992).

6. Concluding remarks

In the experiment on Al wire, we have successfully demonstrated that the new energy-dispersive powder diffraction diffractometer is a viable method for texture studies. With the *PINCER* software installed, the technique is automated and yields texture information rapidly. In addition, it has the capability to probe deeper into the sample with energetic X-rays. If there is a contrasting texture between the surface and the bulk, the results obtained should show the difference. Having established the viability of this technique, we further studied the pole figures of an Er evaporated thin film. The results presented have

shown that the development of strong [002] orientation is readily seen in a film of 600 nm thickness. Results in other samples show that texture can be observed down to at least 200 nm thickness (Craib, Player, Rodman & Tang, 1995). Although restricted in energy resolution, the technique can give other information. Examples are the possibility of stress measurement through the variation of d spacing with ψ, and the correlation of orientation with crystallite size, measured through line broadening (Craib *et al.*, 1995).

Although the existing diffraction apparatus has worked satisfactorily it has limitations, in particular, the angular range of the ψ-axis. With a new circle of 180° movement, this will facilitate a more complete texture mapping. On the φ-circle, an additional small sample goniometer with a height adjustment would be very useful to allow the positioning of the sample at the centre of rotation. This is particularly valuable when a small beam (0.2 mm) is to be used on very thin film specimens at low α, as the alignment
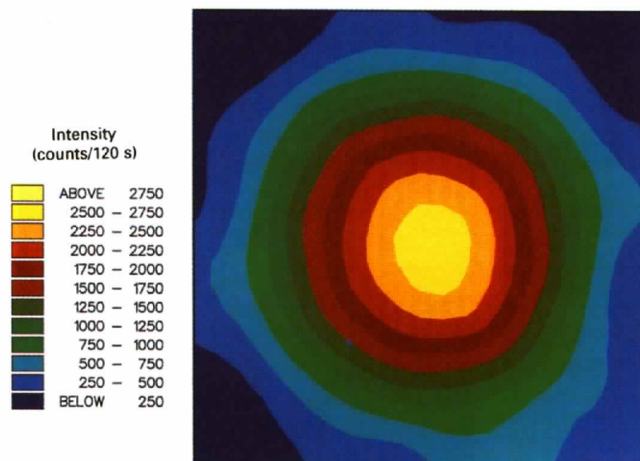

Intensity
(counts/120 s)

ABOVE	2750
2500 –	2750
2250 –	2500
2000 –	2250
1750 –	2000
1500 –	1750
1250 –	1500
1000 –	1250
750 –	1000
500 –	750
250 –	500
BELOW	250

Figure 8
Stereographic plot of Mo $K\alpha$ fluorescence of the substrate.

Intensity
(counts/120 s)

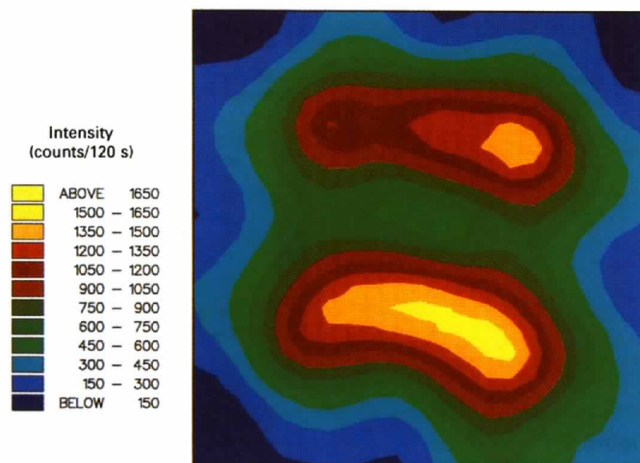|	
ABOVE	1650
1500 –	1650
1350 –	1500
1200 –	1350
1050 –	1200
900 –	1050
750 –	900
600 –	750
450 –	600
300 –	450
150 –	300
BELOW	150

Figure 9
Mo (110) pole figure of the substrate.

becomes more critical. With these considerations in mind, we have already commenced studies for a second design to provide an enhanced texture facility.

References

Barrett, C. S. & Massalski, T. B. (1966). *Structure of Metals*, 3rd ed. New York: McGraw-Hill.

Cernik, R. J., Clark, S. M. & Pattison, P. (1989). *Adv. X-ray Anal.* **33**, 101–107.

Clark, S. M. (1989). *Nucl. Instrum. Methods*, A**276**, 381–387.

Clark, S. M. (1992). *Rev. Sci. Instrum.* **63**(1), 1010–1012.

Clark, S. M. & Miller. M. C. (1990). *Rev. Sci. Instrum.* **61**, 2253–2255.

Craib, G. R. G., Player, M. A., Rodman, M. J. & Tang, C. C. (1995). Presented at the European Powder Diffraction Conference IV, Chester, UK.

Cullity, B. D. (1978). *Elements of X-ray Diffraction*, 2nd ed., ch. 8, pp. 233–323. Reading, MA: Addison-Wesley.

Dillamore, I. L. & Roberts, W. T. (1965). *Met. Rev.* **10**, 271.

Heizmann, J. J., Vadon, A., Schlatter, D. & Bessières, J. (1988). *Adv. X-ray Anal.* **32**, 285–292.

Klug, H. P. & Alexander, L. E. (1974). *X-ray Diffraction Procedures for Polycrystalline and Amorphous Materials*, 2nd ed., ch. 10, pp. 709–754. New York: Wiley–Interscience.

Miller, M. C., Ackroyd, K. S. & Oszlanyi, G. (1994). Daresbury Preprint DL/CSE/P29E and presented at ESONE 8th International Conference on Real Time Data (RT94), Dubna, Russia.

Player, M. A., Marr, G. V., Gu, E., Savaloni, H., Öncan, N. & Munro, I. H. (1992). *J. Appl. Cryst.* **25**, 770–777.